Final publication is available from Mary Ann Liebert, Inc., publishers http://dx.doi.org/10.1089/ars.2015.6402

Original Research Communications

Inhibition of excessive oxidative protein folding is protective in MPP^+ toxicity-induced PD models

Šárka Lehtonen[1], Merja Jaronen[1], Piia Vehviläinen[1], Merja Lakso[1], Martina Rudgalvyte[1], Velta Keksa-Goldsteine[1], Garry Wong[1,2], Michael J. Courtney[1], Jari Koistinaho[1]* and Gundars Goldsteins[1]

[1]Department of Neurobiology, A. I. Virtanen Institute for Molecular Sciences, University of Eastern Finland, P.O. Box 1627, 70211 Kuopio, Finland, [2]Faculty of Health Sciences, University of Macau, China.

Abbreviated title for running head: Protection by PDI inhibition

*Correspondence: Professor Jari Koistinaho, A.I. Virtanen Institute for Molecular Sciences, University of Eastern Finland, P.O. Box 1627, 70211 Kuopio, Finland, jari.koistinaho@uef.fi; tel: +358403552427; fax: +35817163030

Word count: 5651

Reference numbers: 45

Number of grayscale illustrations: 6

Number of color illustrations: 2

Abstract

Aims: Protein misfolding occurs in neurodegenerative diseases including Parkinson's disease (PD). In endoplasmic reticulum (ER) an overload of misfolded proteins, particularly alpha-synuclein (αSyn) in PD, may cause stress and activate the unfolded protein response (UPR). This UPR includes activation of chaperones, such as protein disulphide isomerase (PDI), which assists refolding and contributes to removal of unfolded proteins. While up-regulation of PDI is considered to be a protective response, its activation is coupled with increased activity of ER oxidoreductase 1 (Ero1) producing harmful hydroperoxide. The objective of this study was to assess whether inhibition of excessive oxidative folding protects against neuronal death in well-established MPP^+ models of PD. *Results:* We found that the MPP^+ neurotoxicity and accumulation of αSyn in the ER are prevented by inhibition of PDI or Ero1α. The MPP^+ neurotoxicity was associated with a reductive shift in the ER, an increase in the reduced form of PDI, an increase in intracellular Ca^{2+}, and an increase in Ca^{2+}–sensitive calpain activity. All these MPP^+-induced changes were abolished by inhibiting PDI. Importantly, inhibition of PDI resulted in increased autophagy, and prevented MPP^+-induced death of dopaminergic neurons in *C.elegans*. *Innovation and Conclusion:* Our data indicates that while inhibition of PDI suppresses excessive protein folding and ER stress, it induces clearance of aggregated αSyn by autophagy as an alternative degradation pathway. These findings suggest a novel model explaining the contribution of ER dysfunction to MPP^+-induced neurodegeneration and highlight PDI inhibitors as potential treatment in diseases involving protein misfolding.

Introduction

Parkinson's disease (PD) is a movement disorder with no clear etiology or mechanism. Pathological hallmarks of the disease include the accumulation of α-synuclein (αSyn) into Lewy bodies (LBs) or Lewy neurites and loss of dopaminergic (DA) neurons in the substantia nigra (SN). Previous studies have revealed a central role of αSyn misfolding and oxidative stress in pathogenesis of PD (8, 9).

The presence of misfolded/unfolded proteins disrupts the homeostasis in the endoplasmic reticulum (ER) and triggers the unfolded protein response (UPR) in ER (27) in order to return the ER to its normal physiological balance. Activation of the UPR turns on mechanisms that allow the cell to deal with the accumulated unfolded proteins (11). Mild insults increase the activity of chaperones, such as protein disulfide isomerase (PDI), which assists in correct re-folding and transport of the misfolded/unfolded proteins. Thus, the increased activity of PDI represents an adaptive response induced to protect neuronal cells (16). Importantly, ER homeostasis of DA neurons in the SN is disrupted in PD (21, 31, 37). PDI colocalizes with αSyn in LBs in patients with PD (5). Evidently, the role of the αSyn accumulation-induced ER stress and PDI activation in DA neurons is of great importance.

In ER, PDI catalyzes the formation of disulphide bonds of the misfolded/unfolded proteins (34), which results in reduction of PDI. Re-oxidation of PDI is in turn catalyzed by ER oxidoreductin 1 (Ero1), which produces hydroperoxide (38). An appropriate equilibrium between oxidized and reduced forms of PDI is required for successful oxidative folding (39). Importantly, excessive activation of PDI-Ero1 cycle by an increased influx of misfolded proteins may cause overproduction of hydroperoxide and promote ROS generation (41). Even though the UPR may be a protective response, it thus bears a risk of resulting in detrimental oxidative stress to the cell, including the DA neurons in PD. Alternatively, ER may switch to

autophagy, which, similar to ER stress, can be either protective or promote cell death. Thus, the objective of this study was assess whether inhibition of excessive oxidative folding protects against neuronal death in well-established MPP^+ models of PD, and if so, does a shift to autophagy pathway help coping with the accumulated αSyn.

Results

PDI and Ero1α inhibition increases cell survival of MPP^+-treated SH-SY5Y cells

We first determined MPP^+ toxicity in human neuroblastoma SH-SY5Y cells. Based on the estimated EC50 level, the concentration of 4 mM MPP^+ was selected for further studies (Fig. 1A), which demonstrated that bacitracin and cystamine, well-known PDI inhibitors, increased % of viable cells against MPP^+ -induced cell death in a dose-dependent manner, but showed neurotoxicity at high concentrations. (Fig. 1B, C). Because activation of PDI is coupled with increased activity of ER oxidoreductase 1 (Ero1), we also tested the effect of EN460, a selective and irreversible inhibitor of the active form of Ero1α, and found that EN460 protects against MPP^+ neurotoxicity similar to PDI inhibitors (Fig. 1D).

Bacitracin prevents the accumulation of αSyn

MPP^+ treatment increased expression of αSyn gene *SNCA* and αSyn protein (Fig. 2 D). αSyn and PDI protein expression were also substantially up-regulated upon MPP^+ treatment and showed increased co-localization (Fig. 2 A-B). Bacitracin prevented the αSyn accumulation (Fig. 2 C) and aggregation (Fig. 2 D), and reduced its expression in MPP^+-treated cells at 24 h (Fig. 2 C).

Bacitracin inhibits MPP^+-induced redox shift in the ER

To assess whether MPP^+ alters the highly oxidizing environment in the ER, SH-SY5Y cells were transfected with HyPer probe targeted to the ER lumen and exposed to MPP^+. Flow

cytometry analysis revealed that MPP^+ exposure significantly reduced HyPer probe compared to control cells (Fig. 3 A), indicating a shift in the redox balance in the ER to a more reduced state.

Next, we determined whether the redox state of PDI is also changed upon MPP^+ -induced reduction of the ER environment. Virtually only the oxidized form of PDI was present in control cells (Fig. 3 B), indicating that in the normal ER redox environment Ero1α activity maintains a sufficiently high rate of PDI oxidation. A DTT treatment used as a positive control caused a remarkable induction of reduced form of PDI (Fig 3 B). MPP^+ treatment caused a strong induction of reduced PDI and an increase in total PDI expression (Fig. 3 B-C). Bacitracin significantly suppressed the MPP^+ -induced accumulation of the reduced form of PDI (Fig. 3 B-C). The data suggested that MPP^+ -induced toxicity and αSyn accumulation first activates PDI and even up-regulates its expression but eventually results in accumulation of reduced form of PDI, because in the excessively reduced ER redox environment the capacity of Ero1α to maintain sufficient re-oxidation of PDI appears to be exceeded. By inhibiting over-activation of PDI, bacitracin blocks the reductive shift in the redox state of the PDI and ER environment.

Bacitracin prevents MPP^+-induced increase in intracellular Ca^{2+} and consecutive calpain activation

Over-activation of oxidative protein folding may lead to increased hydroperoxide production, which may cause disruption of the ER Ca^{2+} homeostasis. We found that MPP^+ caused a significant increase in intracellular Ca^{2+} $[Ca^{2+}]i$ (Fig. 4 A), which was blocked by bacitracin. Importantly, the MPP^+-induced increase in $[Ca^{2+}]i$ was totally abolished with 2-APB, an inhibitor of inositol trisphosphate receptors (IP_3R) (Fig. 4 A), which also increased the

viability of MPP^+-treated SH-SY5Y cells (Fig. 4 B). Moreover, the MPP^+-induced elevation in $[Ca^{2+}]i$ led to calpain activation that was again abrogated by bacitracin (Fig. 4 C). Calpain activation was crucial to the cell death, because co-treatment with ALLN (N-Acetyl-Leu-Leu-Norleu-al, N-Acetyl-L-leucyl-L-leucyl-L-norleucinal), a calpain I inhibitor, resulted in increased cell survival (Fig. 4 D). Thus, our data indicated that MPP^+ induces Ca^{2+} release through IP_3R by causing a redox shift and hydroperoxide production in the ER, eventually leading to calpain-mediated cell death.

Bacitracin induces autophagy in MPP^+-treated cells

To find out whether the observed ER stress induced by MPP^+ treatment could lead to autophagy, and whether the autophagy would be affected by PDI inhibition, we analyzed the formation of autophagic vacuoles and expression of proteins associated with autophagy in SH-SY5Y cells. By using monodansylcadaverine (MDC) as a fluorescent probe of autophagy, we observed a trend towards increased number of autophagic vacuoles already after an 1-hour treatment with MPP^+ (Fig. 5 A). The fluorescent signal of MDC appeared stronger after co-treatment with MPP^+ and bacitracin. Quantification of MDC fluorescence intensity showed that while MPP^+ treatment tended to increase the formation of autophagic vacuoles in SH-SY5Y cells (Fig. 5 A), bacitracin alone or in combination with MPP^+ resulted in increased MDC fluorescence intensity (Fig. 5 A). To confirm the autophagy induction by inhibiting PDI, we analyzed the expression of two autophagy-related proteins: p62 that is commonly found in LBs and autophagy inclusions becoming degraded in lysosomes, and B-isoform of human light chain 3 (LC3B), which is converted from LC3B-I to LC3B-II during autophagy. Immunocytochemistry revealed a clear redistribution of p62 into punctuate, vesicle-like structures after MPP^+ treatment (Fig. 5 B), whereas bacitracin alone or in

combination with MPP^+ appeared to result in reduced p62 immunoreactivity. Quantitative immunoblot analysis demonstrated that bacitracin treatment alone or in combination with MPP^+ decreased the amount of p62 and LC3B-I proteins, whereas the amount of LC3B-II protein tended to be increased (Fig. 5 C). These data indicated that inhibition of PDI by bacitracin promotes autophagy in SH-SY5Y cells.

Bacitracin protects against MPP^+-induced dopaminergic neurodegeneration in C. elegans

We next investigated the survival of DA neurons after MPP^+ treatment in *C. elegans* by measuring GFP fluorescence intensity of DA neurons in an integrated strain Is11-7 [$P_{dat\text{-}1}$::GFP]. A 48-h treatment with MPP^+ (0.25-1 mM) induced a dose-dependent decrease in GFP fluorescence intensity, reflecting the survival of the six DA neurons located in the head (Fig. 6 A), as measured by BD Pathway 855 High-Content Image (Fig. 6 C). While the DA neurons of the worms in control wells had fluorescent cell bodies sending out visible and continuous neurites, the DA neurons of the MPP^+-treated worms had shrunken cell bodies and fragmented or thinner neurites that were frequently barely visible (Fig. 6 A). Moreover, the motor functions of the nematode were altered by MPP^+ treatment as the worms exposed to MPP^+ frequently adopted a coiled posture which was never observed in controls (Fig. 6 B). Also, higher concentrations of MPP^+ resulted in slow, less extensive movements of the worms, resembling the akinesia observed in rodent models of PD and patients with PD (Fig. 6 D).

To address the question whether PDI inhibitors protect *C. elegans* against MPP^+-induced DA neurodegeneration, we treated the worms with 0.75 mM MPP^+ in the presence of bacitracin or cystamine. Already at a concentration of 0.5 mM and 0.3 mM respectively, both PDI inhibitors significantly protected the nematodes from MPP^+-induced damage of DA neurons

(Fig 6 C). In addition, bacitracin or cystamine-treated worms showed improved mobility without coiling (Fig. 6 B, D), indicating that MPP^+-induced phenotype can be ameliorated by both inhibitors.

Pdi1 knock down protects against MPP^+-induced dopaminergic neurodegeneration in C. elegans

To determine whether *pdi1* expression plays a role in MPP^+-induced toxicity, an RNAi experiment was performed to knock down its mRNA expression (Fig. 7 A). Our study showed that decreased expression of *pdi1* resulted in significant protection of DA neurons from MPP^+-induced damage (Fig. 7 B).

Discussion

ER is considered to be the quality control core for protein folding. Only correctly folded proteins are transported to their final destination, whereas misfolded and unassembled proteins are retained in the ER (39). To promote correct disulphide bond formation in these misfolded/unfolded proteins (41), the redox environment in the ER is maintained oxidative (22). All the widely used toxins to model PD, such as MPP^+ (an active form of MPTP), 6-hydroxydopamine and rotenone, induce ER stress and activate the UPR in cultured neuronal cells (20, 36, 45) and experimental animal models (37). While 6-OHDA induces multiple targets of UPR, MPP^+ is restricted to the pancreatic ER kinase (PERK) pathway (20). Phosphorylated PERK was found to co-localize with increased cytosolic αSyn in neuromelanin containing dopaminergic neurons of PD cases (21). The presence of pPERK together with αSyn and/or αSyn positive Lewy bodies suggests a functional connection between αSyn pathology and the occurrence of ER stress. Although PDI is induced to maintain normal ER homeostasis during mild stress (29) and it most likely regulates the αSyn accumulation in PD, severe toxic insults appear to overload PDI resulting in redox misbalance and hydroperoxide production in the ER (33). Our data suggest that these reactions in the ER may have fatal consequences such as massive release of intracellular Ca^{2+} via IP_3Rs and activation of calpain, leading eventually to apoptosis.

Our results are in agreement with a previous study on a PC12 cell model of Huntington's disease that showed capability of PDI inhibitors to suppress the apoptosis induced by misfolded proteins (19). Our data extent these findings on beneficial effect of PDI inhibition to human cell model of PD and show further that inhibition of PDI is coupled with consecutive enhancement of autophagy. Considering that PDI and αSyn co-localize in LB and ER of SNpc in post-mortem human brains of PD subjects (5, 21), and that ER stress is a well-described feature of cellular and animal models of PD, our data indicating a key role of reduced and oxidized forms of PDI in neuronal survival may have clinical relevance and improve our understanding of the importance of proper redox environment in the ER, especially in diseases involving misfolded and accumulation proteins.

Similar to the previous studies on DA neurons (34, 43) and neuroblastoma cells (14, 25, 26), we found that MPP^+ induces a dose-dependent accumulation of αSyn into the ER of human neuroblastoma SH-SY5Y cells. The fact that the aggregated αSyn co-localized with PDI in these cells treated with MPP^+ further supports the notion that this ER chaperone may be a major regulator of αSyn accumulation.

Our study demonstrates for the first time that bacitracin, a peptide antibiotic that inhibits reductive activity of PDI by disulphide bond formation (10), protects DA neurons of *C. elegans* from MPP^+ toxicity. While a clear improvement in neuronal viability was achieved by bacitracin presumably via prevention of protein refolding in ER and subsequent induction of autophagy, the bell-shaped dose-response curve of bacitracin in MPP^+-treated cells as well as in *C. elegans* indicates that inhibition of excessive refolding by this peptide may have also an adverse effect on cell survival. Similar protection with a bell-shaped dose-response curve

was seen after treatment with cystamine, another PDI inhibitor, and these results were also in line with an inhibitor of Ero1α.

The MPP^+-induced ER stress was associated with accumulation of αSyn in the ER and ER redox misbalance. Whether the reductive shift in the ER is mediated by αSyn accumulation remains unclear. However, our data supports the notion that the excessive load of αSyn may strongly contribute to the ER redox misbalance, since 1) MPP^+ induced a prominent reductive shift in the ER lumen as assayed with a redox sensitive fluorescence probe, 2) MPP^+ induced a shift from oxidized PDI form to reduced form and also increased the expression of PDI, 3) inhibition of Ero1α, an enzyme regulating re-oxidation rate of PDI and thus its redox state, protected against MPP^+-induced neurotoxicity.

Disruptions in ER Ca^{2+} homeostasis have been associated with many neurodegenerative diseases including PD (21, 32, 33). ER Ca^{2+} depletion leads to the accumulation of unfolded/misfolded proteins in the ER lumen, thereby causing ER stress. In agreement with previous studies, we observed that the treatment with MPP^+ triggered an increase in $[Ca^{2+}]i$ in SH-SY5Y cells, and moreover, that this change in calcium levels was associated with activation of calpain, a Ca^{2+}-sensitive non-lysosomal protease that has been reported to have a disruptive role in SN of PD patients as well as in experimental PD animals (6). Importantly, the MPP^+-induced release of $[Ca^{2+}]i$ was blocked not only by 2-APB, an inhibitor of IP_3R, but also by bacitracin, and promoted cell survival. In addition, ALLN, a calpain I inhibitor, protected neurons from MPP^+ toxicity. These results strongly support the notion that PDI activation is an event upstream to intracellular calcium increase and calpain I activation in our cell model and possibly in *C. elegans* model of PD. Our findings also suggest that the

over-activation of protein oxidative refolding may trigger disruption of calcium homeostasis in the ER with deleterious consequences.

When considering the therapeutic approaches for curing the proteinopathy linked to neurodegenerative diseases such as PD, it is crucial to define whether it is beneficial to facilitate the ER-associated refolding or to support the switch to an alternative protein clearance pathway e. g. autophagy. A recent study by Fouillet et al. (13) showed that mild ER stress, caused by treatment with tunicamycin increased neuronal survival in genetic and pharmacological models of PD through autophagy induction. A similar phenomenon has been detected in other neurodegenerative diseases (18, 42), cardiomyopathy (17), diabetes (44) and cancer (3). We thus hypothesize that during the ER stress autophagy is turned on to support cell survival. Our evidence for bacitracin-induced autophagy in neuroblastoma cell model suggests that this peptide carries out the beneficial effect at least in part via activation of autophagy.

We suggest a novel model explaining the contribution of ER dysfunction to MPP^+-induced neurodegeneration (Fig. 8). Under severe ER stress, inhibition of PDI or Ero1α shifts the redox state and reduces oxidative protein folding in the ER. The prevention of protein refolding by PDI inhibition activates autophagy clearance pathway. The moderate degree of protection by PDI inhibition seen in our studied models is most likely due to mitochondrial toxicity of MPP^+ that remains unattenuated. Nevertheless, inhibition of PDI consistently supports the neuronal survival in our models, indicating that ER stress is a relevant mechanism of the complex action of neurotoxins such MPP^+. Even though the experimental models used in this study are limited to MPP^+ neurotoxicity, our data may explain the previously observed protection by PDI inhibitors in other models of neurodegenerative

diseases (19). Inhibition of excessive protein folding may provide a rationale that links other proteinopathies with ER malfunction.

In summary, inhibition of PDI and the consecutive enhancement of autophagy protected against the MPP^+ -induced protein aggregation and ER dysfunction. The dose response curve of bacitracin was bell-shaped, indicating that excessive prevention of refolding may eventually also compromise cell survival. To harness the regulation of PDI activity for therapeutic purposes, it is critically important to determine whether it is the ER associated refolding or the switch to alternative protein clearance pathways e. g. autophagy that should be pharmacologically supported.

Innovation

We found that the accumulation of α-Synuclein (αSyn) and death of dopaminergic neurons induced by MPP^+, a neurotoxin associated with Parkinson's disease (PD), are prevented by inhibition of protein disulfide isomerase (PDI) or ER oxidoreductase-1. Inhibition of PDI also prevented the MPP^+-induced reductive shift in the ER, increase in the reduced form of PDI, increase in intracellular Ca^{2+} and Ca^{2+}–sensitive calpain activity. Importantly, inhibition of PDI resulted in increased autophagy. These findings suggest a novel model explaining the contribution of ER dysfunction to MPP^+-induced neurodegeneration and highlight PDI inhibitors as potential treatment in diseases involving protein misfolding.

Materials and Methods

Cell culture and cell viability assay

SH-SY5Y (human neuroblastoma) cells were cultured in DMEM/F12 (Lonza) supplemented with 10% heat-inactivated fetal bovine serum (FBS) and 1% v/v penicillin/streptomycin (Lonza) in a humidified incubator containing 5% CO_2 at 37˚C. Cells were passaged every 4 days and used between passages 25 and 35.

Cellular viability was assessed using resazurin (7-Hydroxy-3*H*-phenoxazin-3-one 10-oxide; Sigma-Aldrich) assay. Resazurin is a blue dye –weakly fluorescent until it is reduced to the pink colored and highly red fluorescent resorfin. The human neuroblastoma cells were plated into 96-well plate overnight. The cells were exposed to MPP^+ alone or in the presence of bacitracin (Sigma-Aldrich), cystamine (both from Sigma-Aldrich), ALLN (Millipore) or 2-APB (Sigma-Aldrich). Four or twenty-four hours later, 100 µl fresh medium containing 10 µM resazurin was added into the wells, and the cells were incubated for 2 h at 37 °C. The absorbance was read with Wallac Victor microplate reader (Perkin Elmer). The data are expressed as % of control.

RNA isolation and RT-qPCR

The cell samples were collected and RNA extracted with Tri-Reagent (Sigma-Aldrich) using Nucleospin RNA kit (Macherey-Nagel). cDNA synthesis was performed using random hexamer primers and Maxima reverse transcriptase (Thermo Scientific). The expression level of αSyn was measured according to the manufactures protocol with quantitative real time PCR (StepOnePlus™ Real-Time PCR Systems, Applied Biosystems) using specific assays-on demand target mixes (Life technology). The expression levels were normalized to β-actin and presented as fold change in the expression versus control.

The worms were collected from the plates using M9 buffer and RNA extracted with Trizol solution (Gibco-BRL) immediately. cDNA synthesis was performed using Maxima reverse transcriptase (Thermo Fisher Scientific). Gene specific oligonucleotide primers for RT-qPCR were designed using Primer- BLAST (Ye et al. 2012) and obtained from Oligomer OY (Helsinki, Finland). For amplification reactions Maxima SYBR green qPCR Master mix (Thermo Fisher Scientific) was used and reactions were performed in iCycler 1.0 system (Biorad, Hercules). The expression levels of *pdi1* were normalized to *act-1* and presented as fold change in the expression versus control (worms grown on RNAi plates containing empty vector L4440). Oligonucleotide sequences for PCR were: *act-1-5'*- TCGGTATGGGACAGAAGGAC; *act-1-3'*- CATCCCAGTTGGTGACGATA; *pdi-1-5'*- GTGCTTGTTCTCACTGAAAGC;*pdi-1-3'*- CGTACTTTGGAGCAAGAGAC.

Immunocytochemistry

The treated cells were fixed with 4% PFA for 20 min, permeabilized with 0.25% Triton X-100 and blocked for 60 min with 5% normal goat serum-PBS. Subsequently, cells were incubated with antibody against α-synuclein (mouse monoclonal, BD Transduction Laboratories; 1:300), PDI (rabbit, Assay Designs, 1:300) and anti-SQSTM1 (Santa Cruz Biotechnologies, 1:300) overnight at 4˚C. For visualization of the primary antibodies,

incubation with Alexa Fluor goat-anti mouse 568 and goat anti-rabbit 488 secondary antibodies (1:300) was followed by 4',6-diamidino-2-phenylindole (DAPI) staining.

For quantification of immunoreactive areas and co-localization the coverslips were imaged using a Zeiss LSM 700 confocal microscope (Zeiss Inc., Maple Grove, USA) with an attached digital camera (Color View 12 or F-View; Soft Imaging System, Munster, Germany) running Zen 2009 Image analysis Software (Zeiss Inc., Maple Grove, USA). For the quantification of co-localization, an overlap coefficient and weighted co-localization coefficient parameters were used. The overlap coefficient is a parameter used to quantify co-localization in image pairs and its values range from 0 to 1 (0 = no co-localization, 1 = all pixels co-localize). The weighted co-localization coefficient parameter shows the sums of intensities of co-localizing pixels in channel 1 or 2, respectively, as compared to the overall sum of pixel intensities above threshold and in this channel. Its values range from 0 to 1 (0 = no co-localization, 1 = all pixels co-localize). To quantify the immunoreactive area single stained cells were imaged with Olympus AX70 microscope (Olympus) with attached digital camera (Color View 12, Soft Imaging System, Munster, Germany) running AnalySIS software (Soft Imaging System). Images were further on quantified with ImagePro Plus software (Media Cybernetics, Silver Spring, MD, USA). The data were analyzed using Student's *t* test or ANOVA when appropriate with GraphPad Prism, and *$p < 0.05$, **$p< 0.01$ were considered statistically significant.

Immunoblotting

Cells were collected directly in growing media, washed once with PBS and lysed in 1xLaemmli buffer. The equal loading of the samples was determined by Coomassie staining, and comparable amounts of the protein were run on 8, 10 or 12 % SDS-PAGE gels and transferred to PVDF using Mini Trans-blot Electrophoretic Transfer Cell equipment (Bio-

Rad). Membranes were then blocked and incubated with primary antibodies: anti-PDI (Assay Designs, 1:1000), anti-calpain 1 large subunit (Cell Signaling, 1:1000), anti-SQSTM1 (Santa Cruz Biotechnologies, 1:1000), anti-LC3B (Cell signaling, 1:1000) or anti-β-actin (Sigma Aldrich, 1:2000) overnight at 4˚C. For direct fluorescence detection, the membranes ware incubated for 2 h with Cy5-conjugated secondary antibodies (anti-mouse or anti-rabbit (dilution 1:800, Jackson Immuno Research). Alternatively, the membranes were incubated 2 h with horse radish peroxidase-conjugated antibodies (anti-mouse IgG, dilution 1:4000, anti-rabbit IgG, dilution 1:3000, Amersham Biosciences or anti-goat IgG, dilution 1:2000, Dako) and developed using enhanced chemiluminescence (ECL-kit, GE Healthcare). Membranes were visualized on Storm 860 Fluoroimager (GE Healthcare) and quantified with ImageQuant (Molecular Dynamics, GE Healthcare).

In order to study the redox state of PDI, cell samples were prepared as previously (15). Cells exposed to 10 mM dithiotreitol (DTT; Sigma-Aldrich) for 30 min were used as a positive control. Briefly, cells were washed with ice cold PBS containing 1 mM EDTA and 20 mM N-Ethylmaleimide (NEM; Sigma-Aldrich). Cells were harvested with Triton buffer (20 mM HEPES [pH 7.5], 150 mM NaCl, 1% Triton X-100, 10% glycerol, 1 mM EDTA, 10 mM tetrasodium pyrophosphate, 100 mM sodium fluoride, 17.5 mM β-glycerophosphate, 1 mM phenylmethysulfonyl fluoride, 4 μg/ml aprotonin and 2 μg/ml pepstatin A) supplemented with 20 mM NEM. The equal loading of the samples was determined by Coomassie staining, and comparable amounts of the protein were run on a nonreducing SDS-PAGE and immunoblotted with antiserum to PDI.

To detect the aggregated α-synuclein, cells were washed twice with ice-cold PBS, collected into the phosphate buffer (50 mM) and centrifuged at 3000 rpm for 15 min. Pellets were lysed in 1xLaemmli buffer and applied to a SDS-PAGE gel with a 15% (w/v) acrylamide separating gel. After transfer to PVDF membrane, the blot was incubated with the α-

synuclein antibody (mouse monoclonal, BD Transduction Laboratories; 1:1000) and immunoreactivity was visualized by chemiluminescence using HRP-coupled goat-anti-mouse antibody.

Assessment of redox state of the endoplasmic reticulum

Genetically coded fluorescence probe HyPer targeted to the lumen of ER (12) was used to determine the effects of MPP^+ treatment on the redox state of the ER. Originally, the HyPer probes were designed to detect H_2O_2 in the cell (1) but the ER lumenal HyPer has been suggested to serve as a tool to examine the redox homeastasis of the ER. For this purpose, cells were transfected with ER-targeted HyPer using Lipofectamine 2000 transfection reagent (Invitrogen). Briefly, the Lipofectamine-DNA complexes were formed and mixed with the cells suspended in antibiotic free medium at the desired density. Cells with complexes were plated on 12-well plate and the transfection was performed overnight. Next day, fresh media was changed on the cells. The MPP^+ treatment (4 mM) was started 48 h after transfection and lasted for 24 h. Then the cells were collected by trypsinization and diluted to PBS. HyPer fluorescence was analyzed by flow cytometry (FACS Calibur, BD Biosciences, Franklin Lakes, NJ, USA) using 488 nm Argon laser.

Calcium measurement

Fura-2 (Molecular probes) was loaded into cultured SH-SY5Y at 5 μM with 0.002% pluronic F-127 in DMEM/F12 for 1 h at 37°C. Cultures were washed twice and imaged in Mg^{2+}-free Locke's buffer. Fura-2 responses were measured with 340 nm/ 380 nm excitation and 515 nm/30 nm emission filters using an Olympus Cell^R system. For the excitation ratios corrected background, which normalizes for differences in dye loading between cells are shown. At least 15 cells for each condition was determined in three independent experiments.

Assay to assess autophagy induction

The treated cells were loaded with monodansylcadaverine (MDC; Sigma-Aldrich) for 30 min at 37°C to label autophagic vacuoles. Cultures were washed twice with PBS and imaged by Olympus IX81 (excitation wavelength was set to 335 nm and emission wavelength to 525 nm). Images were further on quantified with ImagePro Plus software. The quantified area was normalized to the number of cells per image. The data are expressed as % of control.

Worm culture and MPP^+ model

Transgenic *C. elegans* integrated strain Is11-7 [Pdat-1::GFP] expressing GFP in its genome under the control of dopamine transporter-1 gene (28) was cultivated and maintained according to the standard protocol. The strain was thawn from freezer vials and placed on freshly prepared Nematode Growth Medium (NGM) that have been spread with *Escherichia coli* (*E.coli*) strain OP50 as a food source and allowed to reproduce for several days. Hermaphrodite form of this *C.elegans* strain has eight DA neurons, six located in the head and two in the tail. Prior to experiments the culture was synchronized. The NGM-plates containing a layer of *E. coli* OP50 were inoculated with 4-5 drops of L1 worms and incubated at 15 ^{o}C for 4 days. Growth of nematode strains was daily followed with a stereomicroscope (Nikon SMZ645). To obtain age-synchronized worms, embryos were first isolated by bleaching gravid adults with sodium hypochlorite, 0.5 M KOH. The eggs were rinsed with M9 buffer and allowed to hatch at 20˚C on rotating shaker at 350 rpm for 14 h to reach L1 stage. For an assay, a suspension of L1 worms and defined amount of E. coli strain OP50 in NGM was distributed into 96-well plates. A 40-µl suspension contained an average of 40 animals per well. First, a dose response for ascending concentrations of MPP^+ (MPP^+ iodide, Sigma-Aldrich) was established. Next, a selected MPP^+ dose in the presence or absence of

bacitracin or cystamine was added to the plates and incubated at 20˚C for 48 h in humidity chamber on rotating shaker.

Assessment of neurodegeneration in worms

Worms were anaesthetized by addition of sodium azide (Sigma-Aldrich) to a concentration of 14 mM. Plates were imaged with a BD pathway 855 High-Content Imager (Becton Dickinson Biosciences) with 10x objective acquiring 25 contiguous fields per well under control of Attovision software (Becton Dickinson Biosciences). The number of worms analyzed per treatment group was approximately 200. The image montages were segmented by Attovision software in two phases, first to define the cluster of bright GFP-positive DA neurons within the head of the worms, and second to identify individual GFP-positive neurons while excluding fragments of or shrunken neurons. Head regions that do not contain a detectable GPF-positive neuron were excluded. This segmentation algorithm was found to efficiently detect worm heads with intact healthy GFP-positive neurons. The sum of GFP fluorescence intensity from all defined head regions containing the GFP-positive neurons was calculated from each montage, as this was found to be the most sensitive and consistent parameter that we tested as an indicator of MPP^+-induced neurodegeneration. The data are expressed as % of control (vehicle-treated *C. elegans*).

Alternatively, the worms were mounted on glass slides containing 2% agarose and imaged under 20x objective with a conventional fluorescence microscope (Olympus AX70) attached to Olympus Soft Imaging system.

Mobility analysis in worms

The treated worms were placed in individual wells of a 96-well microtiter plate containing 50 µl M9 (22 mM KH_2PO_4, 42 mM Na_2HPO_4, 86 mM NaCl, 1mM $MgSO_4.7H_2O$). After a 10

min exposure period to M9, thrashes were counted at 21°C for 30 s. A single thrash was defined as a complete change in the direction of bending at the mid body. In accordance with accepted practice, during manual thrash counts the data for a particular worm was dropped if the worm remained still for > 10 s, or if the worm was visibly damaged. In order to normalize the data, the mean value of vehicle-treated worms was defined as 100%. The individual values from MPP^+-treated worms in the presence or absence of bacitracin or cystamine were compared to this mean value and presented as % of vehicle-treated worm.

RNA interference and assessment of neurodegeneration in worms

To ensure RNA interference in neurons RNAi-sensitive mutant Is11-7K[dat-1p::GFP; acr-2p::GFP;rrf-3] was used. Strain was obtained from the Caenorhabditis Genetics Center (St. Paul, MA USA) and maintained at 20°C temperature on NGM plates containing OP-50 bacteria according to standard protocols.

RNA-mediated interference (RNAi) experiments were executed using standard NGM plates containing isopropyl β-D-thiogalactoside (IPTG, 1 mM) and ampicillin (100 µg/ml). Plates were seeded either with RNase III-deficient *Escherichia coli* bacteria strain HT115 (DE3), carrying L4440 vector with the gene fragment (*pdi-1*) (GeneService, Source BioScience) or empty vector (Addgene). Bacteria cultures for the RNAi-feeding plates were grown for 17 h in liquid L-Broth medium with 100 µg/ml ampicillin. IPTG (1 mM) was added and cultures were grown for 1 h and spread onto plates. Synchronized L1 stage worms were transferred onto plates containing bacteria either with empty L4440 vector for a wildtype control or $RNAi_{(pdi\text{-}1)}$ fragment to knock down the *pdi-1* gene expression and incubated at 20°C for 48 h. L4 stage worms were transferred onto plates containing MPP^+ (0.75 mM) and exposed for 48 h. for Level of neurodegeneration was measured 48 h later by measuring GFP fluorescence. Worms were washed from the plates with M9 buffer, anesthetized and transferred on a glass slide with the agar pad and imaged under 20x objective with a conventional fluorescence

microscope (Olympus AX70) attached to Olympus Soft Imaging system. At least 15 worms/group were imaged from each experiment and the experiment was repeated three times. Results are presented as mean ± S.D.

Statistical analysis

GraphPad-Prism was used for statistical analysis. Results were tested for significant differences using Student's *t* test or one-way ANOVA with *post hoc* Bonferroni test. Resulting *p* values are shown in figure legends, $p < 0.05$ being considered significant. Data are expressed as mean ± S.D.

Acknowledgements

This work was supported by the Emil Aaltonen Foundation, Waldemar von Frenckells Foundation, The Finnish Parkinson Foundation and the Faculty of Health Sciences, University of Macau. Authors would like to thank Professor Kai Kaarniranta and Anne Seppänen for their support in p62 and LC3B western blotting and Olga Vergun for the technical help with Olympus CellΛR system.

Author Disclosure Statement

No competing financial interests exist.

List of Abbreviation

ALLN	N-acetyl-Leu-Leu-Norleual, N-Acetyl-L-leucyl-L-leucyl-L-norleucinal
2-APB	2-aminoethoxydiphenyl borate
αSYN	alpha synuclein
DA	dopaminergic
DDT	dithiothreitol
EC50	half maximal effective concentration
ER	endoplasmic reticulum
ERO1	ER oxidoreductin 1
GFP	green fluorescent protein
IP3R	inositol-3-phosphate receptor
IR	immunoreactivity
LB	Lewy body
LC3	light chain 3
MDC	monodansylcadaverine
MPP+	1-methyl-4-phenylpyridinium
MPTP	1-methyl-4-phenyl-1,2,3,6-tetrahydropyridine
PCR	polymerase chain reaction
PFA	paraformaldehyde
PD	Parkinson disease
PDI	protein disulphide isomerase
p62/SQSTM1	sequestosome 1
ROS	reactive oxygen species
RT-qPCR	real time quantitative polymerase chain reaction
SNpc	substantia nigra pars compacta
UPR	unfolded protein response

References

1. Belousov VV, Fradkov AF, Lukyanov KA, Staroverov DB, Shakhbazov KS, Terskikh AV and Lukyanov S. Genetically encoded fluorescent indicator for intracellular hydrogen peroxide. *Nat. Methods* 3: 281-286, 2006.
2. Braungart E, Gerlach M, Riederer P, Baumeister R and Hoener MC. Caenorhabditis elegans MPP+ model of Parkinson's disease for high-throughput drug screenings. *Neurodegener. Dis.* 1: 175-183, 2004.
3. Chen P, Cescon M and Bonaldo P. Autophagy-mediated regulation of macrophages and its applications for cancer. *Autophagy* 10: 192-200, 2014.
4. Colla E, Jensen PH, Pletnikova O, Troncoso JC, Glabe C and Lee MK. Accumulation of toxic α-synuclein oligomer within endoplasmic reticulum occurs in α-synucleinopathy in vivo. *J. Neurosci Off. J. Soc. Neurosci.* 32: 3301-3305, 2012.
5. Conn KJ, Gao W, McKee A, Lan MS, Ulmann MD, Eisenhauer PB, Fine RE and Wells JM. Identification of the protein disulphide isomerase family member PDIp in experimental Parkinson's disease and Lewy body pathology. *Brain research* 1022: 164-172, 2004.
6. Crocker SJ, Smith PD, Jakson-Lewis W, Lamba WR, Hayley SP, Grimm E, Callaghan SM, Slack RS, Melloni E, Przedborski S, et al. Inhibition of calpains prevents neuronal and behavioral deficits in an MPTP mouse model of Parkinson's disease. *J. Neurosci Off. J. Soc. Neurosci.* 23: 4081-4091, 2003.
7. Dauer W, Kholodilov N, Vila M, Trillat AC, Goodchild R, Larsen KE, Staal R, Tieu K, Schmitz Y, Yuan CA, Rocha M, et al. Resistence of alpha-synuclein null mice to the parkinsonian neurotoxin MPTP. *Proc. Natl. Acad. Sci USA* 99: 14524-14529, 2002.

8. Dauer W and Przedborski S. Parkinson's disease: mechanisms and models. *Neuron* 39: 4081-4091, 2003.
9. Dawson TM and Dawson VL. Molecular pathways of neurodegeneration in Parkinson's disease. *Science* 302: 819-822, 2003.
10. Dickerhof N, Kleffman T, Jack R and McCormick S. Bacitracin inhibits the reductive activity of protein disulphide isomerase by disulphide bond formation with free cysteines in the substrate-binding domain. *FEBS J.* 278: 2034-2043, 2011.
11. Doyle KM, Kennedy D, Gorman AM, Gupta S, Healy SJM and Samali A. Unfolded proteins and endoplasmic reticulum stress in neurodegenerative disorders. *J Cell Mol Med.* 15(10): 2025-39, 2011.
12. Enyedi B, Varnai P and Geiszt M. Redox state of the endoplasmic reticulum is controlled by Ero1L-alpha and intraluminal calcium. *Antioxid. Redox Signal.* 13: 721-729, 2010.
13. Fouillet A, Levet C, Virgone A, Robin M, Dourlen P, Rieusset J, Belaidi E, Ovize M, Touret M, Nataf s, et al. ER stress inhibits neuronal death by promoting autophagy. *Autophagy* 8: 915-926, 2012.
14. Gómez-Santos C, Ferrer I, Reiriz J, Vinals F, Barrachina M and Ambrosio S. MPP+ increases α-synuclein expression and ERK/MAP-kinase phosphorylation in human neuroblastoma SH-SY5Y cells. *Brain Res.* 935: 32-39, 2002.
15. Harding HP, Zhang Y, Bertolotti A, Zeng H and Ron D. Perk is essential for translational regulation and cell survival during the unfolded protein response. *Mol. Cell* 5: 897-904, 2000.
16. Haynes CM, Titus EA and Cooper AA. Degradation of misfolded proteins prevents ER-derived oxidative stress and cell death. *Mol. Cell* 15: 767-776, 2004.

17. He C, Zhu H, Li H, Zou M-H and Xie Z. Dissociation of Bcl-2-Beclin 1 complex by activated AMPK enhances cardiac autophagy and protects against cardiomyocyte apoptosis in diabetes. *Diabetes* 62: 1270-1281, 2013.

18. Hetz C, Thielen P, Matus S, Nassif M, Court F, Kiffin R, Martinez G, Cuervo AM, Brown RH and Glimcher LH. XBP-1 deficiency in the nervous system protects against amyotrophic lateral sclerosis by increasing autophagy. *Genes Dev.* 23; 2294-2306, 2009.

19. Hoffstrom BG, Kaplan A, Letso R, Schmid RS, Turmel GJ, Lo DC and Stockwell BR. Inhibitors of protein disulphide isomerase suppress apoptosis induced by misfolded proteins. *Nat. Chem. Biol.* 6: 900-906, 2010.

20. Holtz WA and O' Malley KL. Parkinsonian mimetics induce aspects of unfolded protein response in death of dopaminergic neurons. *J. Biol. Chem.* 278: 19367-19377, 2003.

21. Hoozemans JJM, van Haastert ES, Eikelenboom P, de Vos RAI, Rozemuller JM and Scheper W. Activation of the unfolded protein response in Parkinson' s disease. *Biochem. Biophys. Res. Commun.* 354: 707-711, 2007.

22. Hwang C, Sinskey AJ and Lodish HF. Oxidized redox state of glutathione in the endoplasmic reticulum. *Science 257*: 1496-1502, 1992.

23. Jaronen M, Vehviläinen P, Malm T, Keksa-Goldsteine V, Pollari E, Valonen P, Koistinaho J and Goldsteins G. Protein disulphide isomerase in ALS mouse glia links protein misfolding with NADPH oxidase-catalyzed superoxide production. *Hum. Mol. Genet.* 22: 646-655, 2013.

24. Javitch JA and Snyder. Uptake of MPP(+) by dopamine neurons explains selectivity of parkinsonism-inducing neurotoxin, MPTP. *Eur. J. Pharmacol.* 106: 455-456, 1984.

25. Kakimura J, Kakimura Y, Takata K, Kohno Y, Nomura Y and Taniguchi T. Release and aggregation of cytochrome c and alpha-synuclein are inhibited by the antiparkinsonian drugs, talipexole and pramipexole. *Eur. J. Pharmacol.* 417: 59-67, 2001.

26. Kalivendi SV, Cunningham S, Kotamraju S, Joseph J, Hillard CJ and Kalyanaraman B. Alpha-synucelin up-regulation and aggregation during MPP+-induced apoptosis in neuroblastoma cells: intermediacy of transferrin receptor iron and hydrogen peroxide. *J. Biol. Chem.* 279: 15240-15247, 2004.

27. Kaufmann RJ. Stress signaling from the lumen of the endoplasmic reticulum: coordination of gene transcriptional and translational controls. *Genes Dev.* 13: 1211-1233, 1999.

28. Lakso M, Vartiainen S, Moilanen AM, Sirviö J, Thomas JH, Nass R, Blakely RD and Wong G. Dopaminergic neuronal loss and motor deficits in Caenorhabditis elegans overexpressing human alpha-synuclein. *J. Neurochem.* 86: 165-172, 2003.

29. Laurindo FRM, Pescatore LA and de Castro Fernandes D. Protein disulphide isomerase in redox cell signaling and homeostasis. *Free Radic. Biol, Med.* 52: 1954-1969, 2012.

30. Mandel R, Ryser HJ, Ghani F, Wu M and Peak D. Inhibition of a reductive function of the plasma membrane by bacitracin and antibodies against protein disulphide-isomerase. *Proc. Natl. Acad. Sci USA.* 90: 4112-4116, 1993.

31. Matus S, Glimcher LH and Hetz C. Protein folding stress in neurodegenerative diseases: a glimpse into ER. *Curr. Opin. Cell Biol.* 23: 239-252, 2011.

32. Nguyen HN, Wang C and Perry DC. Depletion of intracellular calcium stores is toxic to SH-SY5Y neuronal cells. *Brain Res.* 924: 159-166, 2002.

33. Paschen W and Mengesdorf T. Endoplasmic reticulum stress response and neurodegeneration. *Cell Calcium* 38: 409-415, 2005.

34. Przedborski S, Chen Q, Vila M, Giasson BI, Djaldatti R., Vukosavic S, Souza JM, Jackso-Lewis V, Lee VM and Ischiropoulos H. Oxidative post-translational modifications of alpha-synuclein in the 1-methyl-4-phenyl-1,2,3,6-tetrahydropyridine (MPTP) mouse model of Parkinson's disease. *J. Neurochem*. 76: 637-640, 2001.

35. Rao RV and Bredesen DE. Misfolded proteins, endoplasmic reticulum stress and neurodegeneration. *Curr. Opin. Cell Biol.* 16: 653-662, 2004.

36. Ryu EJ, Harding HP, Angelastro JM, Vitalo OV, Ron D and Greene LA. Endoplasmic reticulum stress and the unfolded protein response in cellular models of Parkinson's disease. *J. Neurosci Off. J. Soc. Neurosci.* 22: 10690-10698, 2002.

37. Selvaraj S, Sun Y, Watt JA, Wang S, Lei S, Birnbaumer L and Singh BB. Neurotoxin-induced ER stress in mouse dopaminergic neurons involves downregulation of TRPC1 and inhibition of AKT/mTOR signaling. *J Clin Invest.* 122(4): 1354-67, 2012.

38. Sevier CS, Qu H, Heldman N , Gross E, Fass D and Kaiser CA. Modulation of cellular disulphide-bond formation and the ER redox environment by feedback regulation of Ero1. *Cell* 129(2): 333-44, 2007.

39. Sevier CS and Kaiser CA. Ero1 and redox homeostasis in the endoplasmic reticulum. *Biochim Biophys Acta.* 1783(4): 549-556, 2008.

40. de Simoni S, Linard D, Hermans E, Knoops B and Goemaere J. Mitochondrial peroxiredoxin-5 as potential modulator of mitochondria-ER crosstalk in MPP+-induced cell death. *J. Neurochem* 125: 473-485, 2013.

41. Tu BP and Weissman JS. Oxidative protein folding in eukaryotes: mechanisms and consequences. *J Cell Biol.* 164: 513-517, 2004.

42. Vidal RL, Figueroa A, Court FA, Thielen P, Molina C, Wirth C, Caballero B, Kiffin R, Segura-Aguilar J, Cuervo AM et al. Targeting the UPR transcription factor XBP1 protects against Huntington' s disease through the regulation of Fox01 and autophagy. *Hum. Mol. Genet.* 21: 2245-2262, 2012.

43. Vila M, Vukosavic S, Jackson-Lewis V, Neystat M, Jakowec M and Przedborski S. Alpha-synuclein up-regulation in substantia nigra dopaminergic neurons following administration of the parkinsonian toxin MPTP. *J. Neurochem.* 74: 721-729, 2000.

44. Yamahara K, Yasuda M, Kume S, Koya D, Maegawa H and Uzu T. The role of autophagy in the Pathogenesis of Diabetic Neuropathy. *J. Diabetes Res.* 2013: e193757, 2013.

45. Zeng X-S, Jia J-J, Kwon Y, Wang S-D and Bai J. The role of thioredoxin-1 in suppression of endoplasmic reticulum stress in Parkinson disease. *Free Radic. Biol. Med.* 67: 10-18, 2014.

Figure legends

Figure 1. PDI inhibition increases cell survival of MPP^+-treated human neuroblastoma SH-SY5Y cells. (A) Dose-response graph of MPP^+-treated cells at 24 h measuring cell survival. The beneficial effects of PDI and Ero1α inhibitors – (B) bacitracin, (C) cystamine and (D) EN460 in 4 mM MPP^+-exposed cells measured by a resazurin assay. Data are expressed as mean % of viable cells ± S.D. One-way ANOVA, *** $p < 0.001$; ** $p < 0.01$; * $p < 0.05$. n =6.

Figure 2. Bacitracin treatment prevents the accumulation of αSyn in MPP^+ -treated SH-SY5Y cells. Figure (A) shows typical examples of confocal images of αSyn (red) and PDI (green) in MPP^+-treated cells. αSyn co-localized with PDI in the ER of SH-SY5Y cells. (B) At 24 h, 4 mM MPP^+-treated cells showed increased levels of PDI immunoreactivity (PDI-IR) in the ER. Data are expressed as mean % of control ± S.D. The overlap coefficient of PDI and αSyn was significantly increased after MPP^+ exposure. In addition, weighted co-localization coefficient of PDI and αSyn revealed significantly higher levels of αsyn after MPP^+ treatment. Data are shown as mean ± S.D. Unpaired two-tailed t-test, ** $p < 0.01$. At least 40 images for each condition were quantified. Scale bar 10 μm. Figure (C) shows typical examples of images of αSyn immunoreactivity in 4 mM MPP^+-treated cells either alone or with 1 mM bacitracin co-treatment at 24 h. Bacitracin-treated cells (1 mM) showed significantly reduced levels of αSyn immunoreactivity (α-synuclein-IR) in the cytosol after

co-treatment with 4 mM MPP^+ (MPP^+) for 24 h. Data are expressed as fold change over control cells ± S.D. One-way ANOVA, *** $p < 0.001$; * $p < 0.05$. n = 6, at least 40 cells for each condition were quantified. Scale bar 10 µm. (D) Representative immunoblots of aggregated α-synuclein (19 kDa) and housekeeping protein β-actin (42 kDa) after 4 mM MPP^+ treatment and co-treatment with 1 mM bacitracine. Quantification of α-synuclein protein expression showed a significant increase in aggregated α-synuclein upon MPP^+ treatment. Bacitracin prevented α-synuclein aggregation. A dose-response effect on *SNCA* mRNA expression levels as measured by quantitative RT-PCR from SH-SY5Y cells after 24 h MPP^+ treatment. Data are presented as mean relative expression normalized to β-actin ± S.D. One-way ANOVA, *** $p < 0.001$; * $p < 0.05$.

Figure 3. MPP^+ treatment causes ER redox misbalance. (A) In SH-SY5Y cells exposed to MPP^+ (gray) the HyPer probe was markedly reduced compared to the untreated cells (black) indicating increased reductive shift in the ER upon MPP^+ treatment as measured by flow cytometry. (B) Representative immunoblots of PDI forms (57 kDa) and housekeeping protein β-actin (42 kDa) after 4 mM MPP^+ treatment and co-treatment with 1 mM bacitracine. Cells exposed to 10 mM dithiothreitol (DTT) for 30 min were used as positive control. (C) Quantification of PDI forms showed a severe increase in ratio of reduced/oxidized PDI upon MPP^+ treatment. Bacitracin suppressed the accumulation of reduced form. Data are expressed as fold change over control ±S.D. One-way ANOVA, * $p < 0.05$. n = 4.

Figure 4. PDI inhibition prevents MPP^+ induced increase in intracellular Ca^{2+} and consecutive calpain activation. (A) MPP^+ treated SH-SY5Y cells showed significantly elevated levels of $[Ca^{2+}]i$ compared to control cells as measured by ratiometric fluorescence

imaging. The increase in $[Ca^{2+}]i$ was abolished by 1 mM bacitracin and 25 μM 2-Aminoethoxydiphenyl borate (2-APB), an inositol triphosphate receptor (IP_3R) inhibitor. Data are expressed as mean % of calcium ± S.D. One-way ANOVA, *** $p < 0.001$. n = 3, at least 50 cells for each condition were analysed. (B) IP_3R inhibition with 2-APB improved SH-SY5Y cell survival after exposure to 4 mM MPP^+. Data are expressed as mean % of viable cells ± S.D. One-way ANOVA, *** $p < 0.001$; ** $p < 0.01$. n = 6. (C) MPP^+ treatment resulted in a significant increase in the calpain activation as measured by expression of active 75 kDa calpain form. This increase was reduced by 1 mM bacitracin. The intensity of 80 and 75 kDa bands were quantified and normalized to loading control (β-actin). Data are shown as fold change over control ±S.D. One-way ANOVA, * $p < 0.05$. n = 4. (D) ALLN, calpain I inhibitor, dose dependently protected MPP^+-induced cell loss. Data are expressed as mean % of viable cells ± S.D. One-way ANOVA, *** $p < 0.001$. n = 6.

Figure 5. PDI inhibition induces autophagy. (A) Representative fluorescence images of autophagic vacuoles stained with monodansylcadaverine (MDC). Bacitracin treatment (1 mM) increased MDC fluorescence intensity in SH-SY5Y cells after 1 h. Data are expressed as mean % of fluorescence intensity ± S.D. One-way ANOVA, * $p < 0.05$. n = 4, at least 40 images for each condition were analysed. Figure (B) shows typical examples of confocal images of αSyn (red) and p62 (green) in 4 mM MPP^+-treated cells. (C) Representative immunoblots of p62 (62 kDa) and LC3B (LC3B-I 16 and LC3B-II 14 kDa) at 4 h. Treatment with 1 mM bacitracin significantly abolished p62-expressed levels and increased LC3B-II expression after treatment with MPP^+ at 4 h. The protein expression levels are presented as mean relative expression normalized to β-actin ± S.D. One-way ANOVA, ** $p < 0.01$; * $p < 0.05$. n = 4. Scale bar 10 μm.

Figure 6. PDI inhibition protects against MPP^+-induced dopaminergic neurodegeneration in *C.elegans* (P_{dat1}::GFP). Representative fluorescence (A) and bright field images (B) of *C.elegans* in liquid culture at 48 h. MPP^+-treated worms exhibited a pronounced phenotype. The worms adopted a coiled posture and their movement was uncoordinated. The DA neurons of the 0.75 mM MPP^+-treated worms appeared to have shrunken cell bodies and fragmented or thinner neurites. (C) A dose dependent effect of MPP^+ treatment on the degeneration of DA neurons in the head of *C. elegans* as assessed by BD Pathway 855 High-Content Imager. Bacitracin and cystamine significantly protected the worms from 0.75 mM MPP^+-induced dopamine neurons loss and improved their mobility (D). Data are expressed as mean % of control (vehicle-treated *C.elegans*) ± S.D. One-way ANOVA, *** $p < 0.001$; ** $p < 0.01$; * $p < 0.05$. $n = 6$.

Figure 7. *PDI1* knock down protects against MPP^+-induced dopaminergic neurodegeneration in *C.elegans.* (A) *PDI1* mRNA expression levels as measured by quantitative RT-PCR from worms feeded either with empty L4440 vector (C-control) or $RNAi_{pdi-1}$ fragment to knock down the *pdi-1* gene expression. Data are presented as mean relative expression normalized to *act-1* ± S.D. (B) $RNAi_{pdi-1}$ significantly protected the worms from 0.75 mM MPP^+-induced dopamine neurons loss assessed by measuring GFP fluorescence. Data are expressed as mean % of control ± S.D. One-way ANOVA, ** $p < 0.01$, * $p < 0.05$. $n = 3$.

Figure 8. A proposed model for the role of PDI and Ero1α inhibition in MPP^+-induced models. Accumulation of misfolded/unfolded proteins like αSyn causes ER stress, a similar effect is seen by treatment with MPP^+. Excessive refolding in the ER upregulates PDI reduced form. Re-oxidation of PDI is linked to dysregulation of IP_3R permeability, causing

an increase in cytosolic calcium followed by calpain activation mediated apoptosis. PDI inhibition by bacitracin prevents ER redox imbalance and downstream pro-apoptotic events. In addition, bacitracin enhances autophagic clearance of aggregated αSyn.

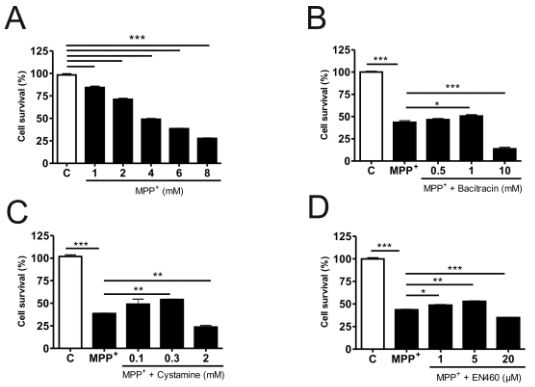

Figure 1

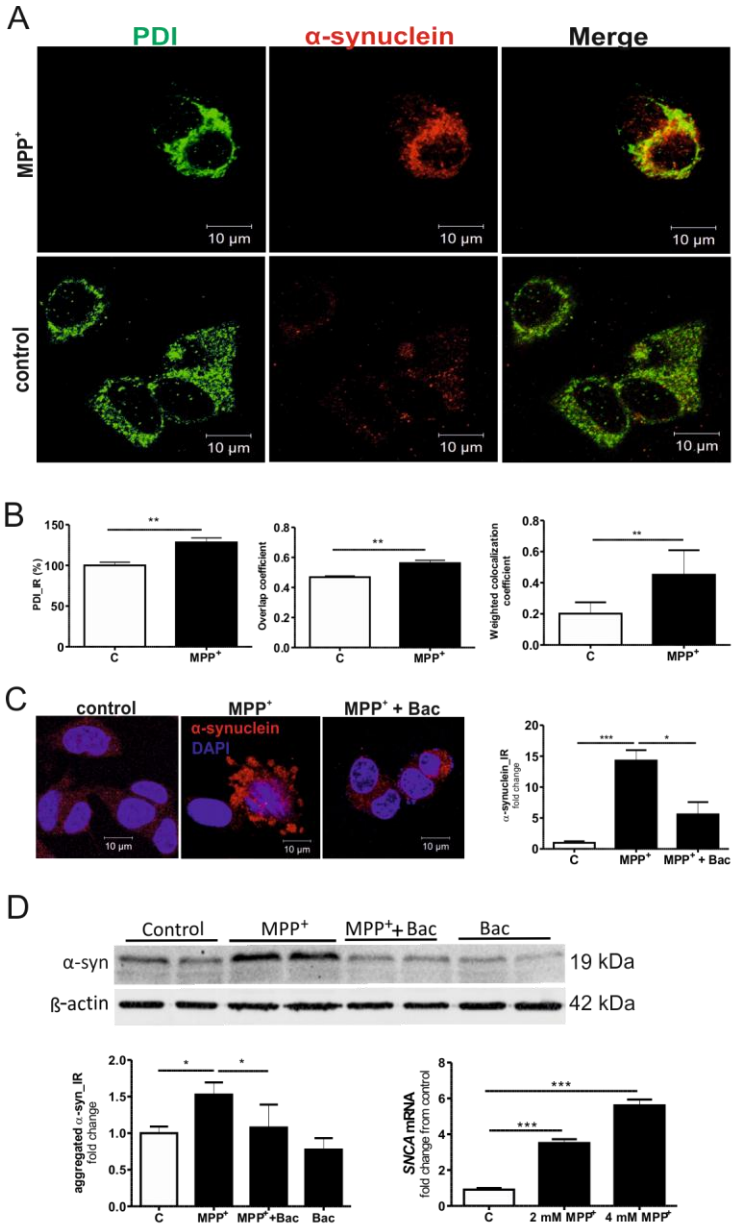

Figure 2

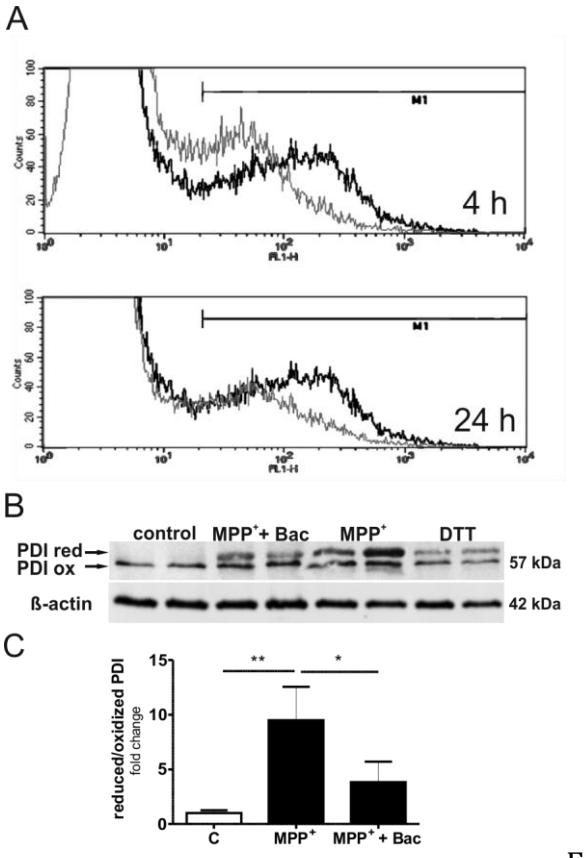

Figure 3

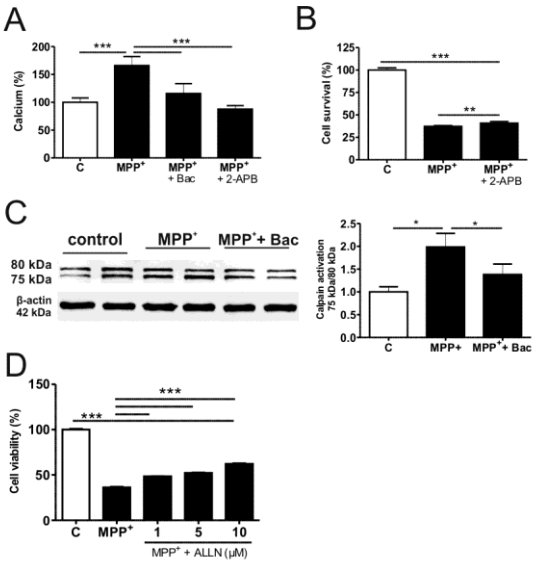

Figure 4

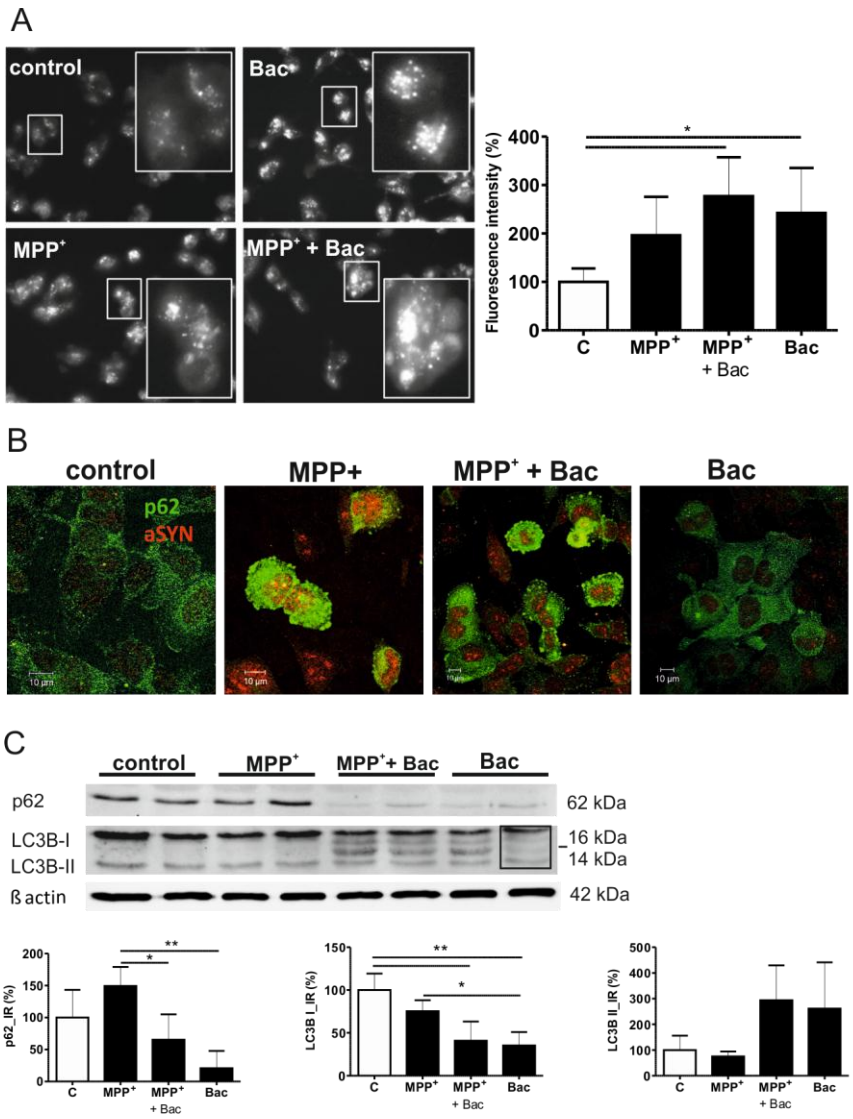

Figure 5

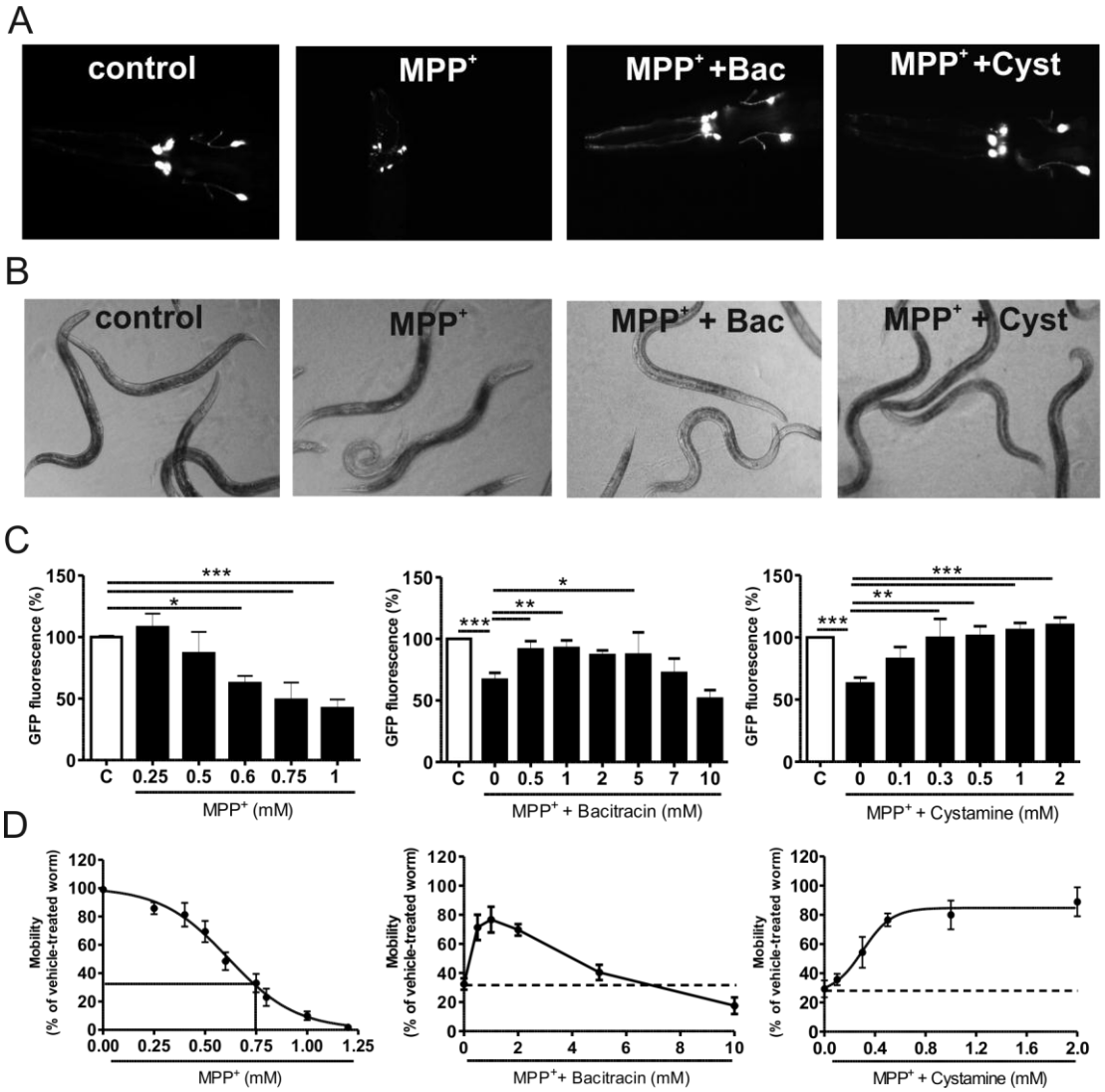

Figure 6

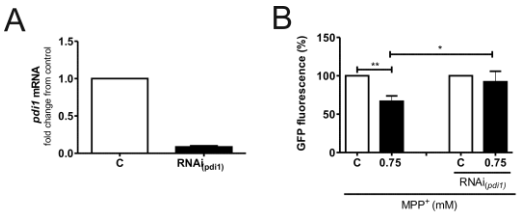

Figure 7

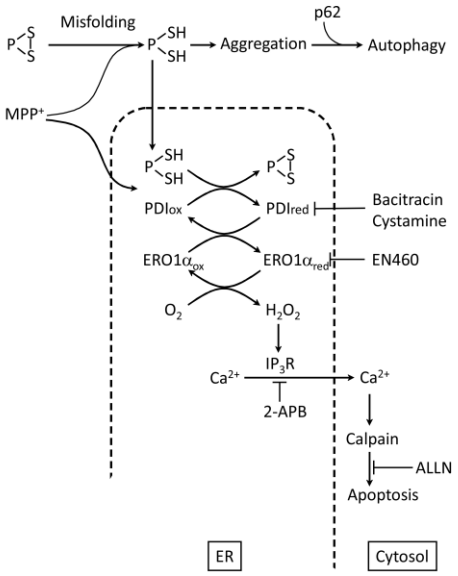

Figure 8

copy of rawdata 25042016.xlsx